Science Bulletin 67 (2022) 655–664

Contents lists available at ScienceDirect

Science Bulletin

journal homepage: www.elsevier.com/locate/scib

Article

# Extreme fire weather is the major driver of severe bushfires in southeast Australia

Bin Wang [a,b,*], Allan C. Spessa [c], Puyu Feng [d], Xin Hou [e], Chao Yue [a], Jing-Jia Luo [f,*], Philippe Ciais [g], Cathy Waters [h], Annette Cowie [i,j], Rachael H. Nolan [k], Tadas Nikonovas [c], Huidong Jin [l], Henry Walshaw [m], Jinghua Wei [f], Xiaowei Guo [n], De Li Liu [b,o], Qiang Yu [a,p,*]

[a] State Key Laboratory of Soil Erosion and Dryland Farming on the Loess Plateau, Northwest A&F University, Yangling 712100, China
[b] New South Wales Department of Primary Industries, Wagga Wagga Agricultural Institute, Wagga Wagga 2650, Australia
[c] Department of Geography, College of Science, Swansea University, Singleton Park, Swansea SA2 8PP, UK
[d] College of Land Science and Technology, China Agricultural University, Beijing 100193, China
[e] College of Natural Resources and Environment, Northwest A&F University, Yangling 712100, China
[f] Institute for Climate and Application Research (ICAR)/Key Laboratory of Meteorological Disaster of Ministry of Education (KLME), Nanjing University of Information Science and Technology, Nanjing 210044, China
[g] Laboratoire des Sciences du Climat et de l'Environnement, CEA-CNRS-UVSQ, Gif sur Yvette F-91191, France
[h] New South Wales Department of Primary Industries, Dubbo 2830, Australia
[i] New South Wales Department of Primary Industries, Armidale 2351, Australia
[j] School of Environmental and Rural Science, University of New England, Armidale 2351, Australia
[k] Hawkesbury Institute for the Environment, Western Sydney University, Penrith 2751, Australia
[l] CSIRO Data61, Canberra 2601, Australia
[m] Python Charmers Pty Ltd, Hawthorn 3122, Australia
[n] Key Laboratory of Adaptation and Evolution of Plateau Biota, Northwest Institute of Plateau Biology, Chinese Academy of Sciences, Xining 810008, China
[o] Climate Change Research Centre, University of New South Wales, Sydney 2052, Australia
[p] College of Resources and Environment, University of Chinese Academy of Sciences, Beijing 100049, China

ARTICLE INFO

*Article history:*
Received 20 July 2021
Received in revised form 7 September 2021
Accepted 8 September 2021
Available online 5 October 2021

*Keywords:*
Remote sensing
Forest fires
Climate drivers
Burnt area modelling
Machine learning
Southeast Australia

ABSTRACT

In Australia, the proportion of forest area that burns in a typical fire season is less than for other vegetation types. However, the 2019–2020 austral spring-summer was an exception, with over four times the previous maximum area burnt in southeast Australian temperate forests. Temperate forest fires have extensive socio-economic, human health, greenhouse gas emissions, and biodiversity impacts due to high fire intensities. A robust model that identifies driving factors of forest fires and relates impact thresholds to fire activity at regional scales would help land managers and fire-fighting agencies prepare for potentially hazardous fire in Australia. Here, we developed a machine-learning diagnostic model to quantify nonlinear relationships between monthly burnt area and biophysical factors in southeast Australian forests for 2001–2020 on a 0.25° grid based on several biophysical parameters, notably fire weather and vegetation productivity. Our model explained over 80% of the variation in the burnt area. We identified that burnt area dynamics in southeast Australian forest were primarily controlled by extreme fire weather, which mainly linked to fluctuations in the Southern Annular Mode (SAM) and Indian Ocean Dipole (IOD), with a relatively smaller contribution from the central Pacific El Niño Southern Oscillation (ENSO). Our fire diagnostic model and the non-linear relationships between burnt area and environmental covariates can provide useful guidance to decision-makers who manage preparations for an upcoming fire season, and model developers working on improved early warning systems for forest fires.

© 2021 Science China Press. Published by Elsevier B.V. and Science China Press. This is an open access article under the CC BY license (http://creativecommons.org/licenses/by/4.0/).

## 1. Introduction

Australia is the driest ice-free continent and is second only to Africa in terms of the total area burnt annually by vegetation fires [1]. Approximately 5% (40 million ha) of the Australian continent burns annually, and all but the most arid parts of the continent

* Corresponding authors.
*E-mail addresses:* bin.a.wang@dpi.nsw.gov.au (B. Wang), jjluo@nuist.edu.cn (J.-J. Luo), yuq@nwsuaf.edu.cn (Q. Yu).

https://doi.org/10.1016/j.scib.2021.10.001
2095-9273/© 2021 Science China Press. Published by Elsevier B.V. and Science China Press.
This is an open access article under the CC BY license (http://creativecommons.org/licenses/by/4.0/).

are susceptible to periodic fire [2]. Fire frequency is particularly high in the tropical savannas of northern Australia, with fire return intervals (FRIs) ranging from one to five years, associated with relatively low intensity fires due to dominance of grass fuels [3]. By contrast, the eucalypt forests and woodlands in south-eastern (SE) and south-western Australia are characterised by much less frequent fires (FRI > 20 years) [2]. While relatively infrequent, southern forest fires nonetheless have potentially more profound social, economic and ecological consequences as they have higher fire intensities and often occur in close proximity to settlements and infrastructure [4].

Driven by a long-term drought in eastern Australia [5], many fires erupted in New South Wales (NSW) in early September 2019. Forest fires rapidly spread from north to south of eastern NSW, and escaped control from September through January despite tremendous efforts at containment from firefighters, landholders, and government. The MODIS Burned Area data products (Terra and Aqua combined MCD64A1 Version 6) show that fires burnt around 5.4 million ha of forestland from September 2019 to February 2020 over NSW and Victoria. More than one billion mammals and birds were killed by the fires, and habitats of up to 100 threatened plant and animal species were destroyed, pushing at least 20 threatened species closer to extinction [6]. Over 350 million tonnes of $CO_2$ were released from bushfires during late 2019 [7], which is around two-thirds of Australia's total annual greenhouse gas emissions [8]. The total area burnt by the forest fires in SE Australia was unprecedented in two decades of recorded history [9,10]. Given that the occurrence of similar climate conditions that preceded such fires is expected to increase under future climate change [5], identifying and quantifying the key drivers of forest fire activity is crucial for improved fire forecasting to inform more effective fire management planning and mitigation.

The incidence of vegetation fires is controlled by many factors including ignition sources (human-caused and dry lightning strikes), fuel availability, fuel moisture, topography, land and forest management, fire suppression, and human settlement patterns. Weather (rainfall, temperature, relative humidity, and wind) is an important driver of the rate of spread and hence area burnt by individual fires [11,12]. Machine Learning (ML) confers several advantages over traditional statistical modelling of ecological phenomena, for example, ML can handle different data types (continuous, categorical); it makes no assumptions about the training data or prediction residuals; it can flexibly capture highly non-linear relationships; and it can accommodate missing data, both in the response and in the predictors [13]. In recent years, several studies have used ML to quantify the links between antecedent environmental conditions including hot, dry weather and burnt area in different regions [14]. For example, Amatulli et al. [15] used a decision-tree based Random Forest (RF) ML model to estimate burnt areas in the European Mediterranean countries with the Canadian Fire Weather Index (FWI). Ma et al. [16] also trained a RF model with the MODIS Global Fire Atlas dataset (2010–2016) to analyse the impacts of climate, topography, vegetation, and socioeconomic variables on forest fire occurrence in six geographical regions in China. In Australia, Dutta et al. [17] and Clarke et al. [18] used Artificial Neural Networks (ANN) to model fire activity. The former analysed fire frequency as a function of climate-related variables on a weekly time step at major climate region/state-wide resolutions; whereas, the latter predicted the probability of large fires (classified as a binary variable based on a 50% burnt area threshold) as a function of fire weather, biomass, fuel moisture, and ignitions on an annual time step at a 5 km resolution. The fire data analysed in both studies were limited up to the years 2013 and 2014, respectively.

There has been a long-term increase in extreme fire weather and in the length of the fire season across SE Australia over the past few decades [19,20]. Although there is considerable inter-annual variability in fire weather conditions in 1973–2017, there is also a clear trend in more recent decades towards a greater number of dangerous bushfire days characterised by severe fire weather [20]. On the other hand, climate projections for the 21st century show significant warming and decreased precipitation over Australia, particularly in SE Australia [21]. These conditions will increase the likelihood of extreme bush fires in the future. The year-to-year changes in SE Australia's climate are mostly associated with three major natural climate modes: the El Niño Southern Oscillation (ENSO) in the tropical Pacific Ocean, the Indian Ocean Dipole (IOD) in the Indian Ocean, and the Southern Annular Mode (SAM) in the southern ocean [22]. The occurrence of prolonged drought in forested areas is conducive for large bushfires [23]. Typically, the most severe drought and bushfire events in SE Australia have been associated with the combination of an El Niño and a positive IOD disrupting the normal spring-summer rainfall patterns [24–26]. The impacts of these climate modes on climate variability in Australia have increased over the recent past and are predicted to be enhanced in the future under anthropogenic warming [27,28]. Numerous studies have used correlation analyses to examine statistical relationships between these climate modes and fire weather in Australia [20,29,30]. However, as far we are aware, few studies have assessed potential non-linear relationships between these modes and extreme fire weather in forested regions of southeast Australia.

Understanding non-linear relationships of fire activity versus biophysical variables in concurrent season is a necessary precursor to developing a fire forecasting system in Australia based on outputs from seasonal climate forecasts and vegetation models. An awareness of such thresholds in biophysical parameters is useful so that fire-fighting resources can be mobilised ahead of time to prepare for potentially hazardous fire conditions several months in advance. Here we aim to develop RF diagnostic models to quantify important non-linear relationships between monthly burnt area and biophysical variables at a resolution of $0.25^\circ \times 0.25^\circ$ across the SE Australia forest region (Fig. S1 online). The partial dependence plot from the RF model can demonstrate how each predictor variable dynamically affects burnt area, which is valuable for identifying thresholds for environmental covariates associated with extreme burnt area. As Australia's climate has a strong teleconnection with large-scale climate modes [22], we also use the RF model to explore the non-linear relationship between the three major climate modes (ENSO, IOD, and SAM) and fire weather indices.

## 2. Materials and methods

### 2.1. MODIS burnt area

Fire activity is represented by burnt area (BA) in this study. BA reflects the outcome of a fire season and integrates ignition events as well as fire weather and fuel characteristics that determine fire spread. Daily BA with 500-m resolution was obtained from the Collection 6 Moderate Resolution Imaging Spectrometer (MODIS) Burned Area product (MCD64A1, https://ladsweb.modaps.eosdis.nasa.gov/search/order/2/MCD64A1-6, accessed 20 May 2020) [1]. We selected data from January 2001 to February 2020. In addition, we used the MODIS Land Cover Type Product (MCD12Q1, https://ladsweb.modaps.eosdis.nasa.gov/search/order/1/MCD12Q1-6) to derive and extract land cover data at 500 m spatial resolution. MCD12Q1 product has been widely used in Australian fire studies [31,32]. We chose this product since it has same resolution as the MODIS Burned Area product. We used the MODIS Land Cover Type Product to extract forest area from the MODIS Burned Area

product, with focus on the southeast Australian forest region. Then we calculated the proportion of area burnt (PAB) on a 0.25° grid for each month in austral spring and summer over 2001–2020.

Annual, seasonal, and spatial variations in burnt area were large, which resulted in a highly positively skewed distribution of observed monthly PAB values over all samples. We restricted our analyses to the main period of forest fire (October–February) to predict non-zero PAB, that is, where at least some fire occurs. In total, there were 3530 samples with non-zero PAB across SE Australian forest areas in 2001–2020.

### 2.2. Fire weather conditions

Analyses of fire weather conditions were based on two main systems: the Canadian Forest Fire Weather Index (FWI) System, which provides a rating of fire danger based on fuel moisture and fire behaviour potential [33,34] (see Section 1 in Supplementary materials), and the McArthur Forest Fire Danger Index [35]. The FWI outputs only depend on daily meteorological parameters and do not consider differences in fuel types or topography, providing a uniform, relative rating of fire danger [33]. The FWI system has six components, viz., three fuel moisture codes (Fine Fuel Moisture Codes (FFMC), Duff Moisture Code (DMC), Drought Code (DC)), and three fire behaviour indices (Initial Spread Index (ISI), Build Up Index (BUI), Fire Weather Index (FWI)). Here we selected FFMC, DC, and FWI to predict historical monthly PAB. The McArthur Forest Fire Danger Index includes the Forest Fire Danger Index (FFDI) and Keetch-Byram Drought Index (KBDI) [34,35].

We downloaded global gridded daily FFMC, DC, FWI, FFDI, and KBDI historical data for the 1979–2020 period from the Copernicus Emergency Management Service (https://cds.climate.copernicus.eu/cdsapp#!/home) which were calculated using weather forecast from historical simulations provided by ECMWF ERA5 reanalysis at a resolution of 0.25° [36]. They were then clipped to the Australian continent. We then calculated gridded monthly means (FFMC_mean, DC_mean, FWI_mean, FFDI_mean, and KBDI_mean) and the number of days when daily FFMC, DC, FWI, FFDI, KBDI respectively exceeded the 90th percentile for each individual month in September−February (FFMC90, DC90, FWI90, FFDI90, and KBDI90).

### 2.3. Land use and vegetation

The catchment scale land use of Australia was downloaded from the Australian Bureau of Agricultural and Resource Economics and Sciences (ABARES, https://www.agriculture.gov.au/abares). There were six primary and 33 secondary classifications according to the Australian Land Use and Management (ALUM) Classification version 8 (https://www.agriculture.gov.au/sites/default/files/abares/aclump/documents/clum_data_2018/CLUM_map_December2018_ALUM_secondary.pdf). We calculated the percentage of area under settlements and water (urbanization and water ratio, UW_ratio), and the percentage of forests (forest ratio, F_ratio) at each 0.25° grid cell.

The fractional cover of Photosynthetic Vegetation (f_PV, including green plants), Non-Photosynthetic Vegetation (f_NPV, including dry vegetation and dead woody material) and bare soil (including stones and rock) are critical variables influencing bushfire occurrence and spread. Both PV and NPV represent opposing yet complementary indicators of flammable fuel availability [37]. The monthly product of Vegetation Fractional Cover with 500 m spatial resolution is derived from the MODIS Nadir BRDF-Adjusted Reflectance product (MCD43A4) collection 6, starting from January 2001 and actively maintained by the Earth Observation Landscapes team, CSIRO (https://eo-data.csiro.au/remotesensing/v310/Australia/monthly/cover/). MODIS fractional cover data have been validated in Australia [38] and previous studies have used this product to estimate soil properties [39]. Given that f_PV and f_NPV had a strong correlation ($R^2$ = 0.88), we selected average f_NPV for the current month and the previous month to represent fuel flammability in each month at 0.25° across the SE Australian forest areas.

Long-term trend in Normalised Difference Vegetation Index (NDVI) has been shown to reflect changes in biomass or fuel load through time and space [40–42]. We used monthly average NDVI with a 5 km spatial resolution from Australia Bureau of Meteorology (http://www.bom.gov.au/jsp/awap/ndvi/index.jsp). These NDVI data are computed from signals received from the Advanced Very High Resolution Radiometer (AVHRR) instruments on board the National Oceanic and Atmospheric Administration (NOAA) series of satellites. We used MODIS Land Cover Type Product to extract NDVI for forest vegetation and resampled NDVI data at 0.25° resolution. To capture biomass availability for each 0.25° grid cell, we calculated the median of the 60 monthly average AVHRR-derived NDVI values that preceded the fire season for that grid cell over the past five years. This method follows Zhang et al. [40] who demonstrated a close link between long-term NDVI, biomass availability and fire occurrence in SE Australian forests, and Guerschman et al. [43] who reported a close relationship between 60 months antecedent rainfall and vegetation cover across Australia. We used long-term AVHRR-derived NDVI rather than MODIS-derived NDVI because the latter only started when the MODIS-derived BA record commenced in 2001. We conducted a sensitivity analysis of the impact of choosing different period lengths (1–6 years) on our results but found no discernible effect on model performance. We were unable to explore longer periods because there is a cluster of missing values from AVHRR satellite across our study region in the mid-1990s (http://www.bom.gov.au/climate/austmaps/about-ndvi-maps.shtml).

### 2.4. Climate drivers

There are three major climate drivers influencing Australia's climate: the Southern Annular Mode, the El Niño–Southern Oscillation (ENSO), and the Indian Ocean Dipole (IOD). SAM describes the north–south movement of the westerly wind belt circling Antarctica and is an important indicator of rainfall in southern Australia. We used an observation-based monthly SAM dataset based on Marshall [44] (http://www.nerc-bas.ac.uk/icd/gjma/sam.html). The IOD is the difference in sea surface temperatures in the tropical western and eastern Indian Ocean. It has widespread impacts on precipitation in countries surrounding the Indian Ocean, including India, Indonesia, and Australia [26]. Monthly IOD series for the study period were downloaded from JAMSTEC (http://www.jamstec.go.jp/virtualearth/general/en/index.html). There are a few indicators used for measuring ENSO, such as Southern Oscillation Index (SOI, a measurement of the anomalies of sea level pressure from Darwin and Tahiti) and sea surface temperatures (SST) in the tropical Pacific Ocean (Niño 3 and Niño 4). El Niño is a negative phase of SOI and Australia usually experiences less rainfall in El Niño years [45]. During year-to-year El Niño events in recent decades, major sea surface warming has occurred frequently in the central Pacific (CP), which is different from the eastern Pacific (EP) warming pattern [46]. We used a transformed index to represent SST in the central Pacific Ocean (CP = Niño4 – 0.5Niño3) and eastern Pacific (EP = Niño3 – 0.5Niño4) El Niño events [47].

### 2.5. Random forest model and variable importance

To assess the interactions between environmental features and burnt area, we used the Random Forest (RF) model [48], which has been extensively adopted in ecological studies to analyse complex

systems, including modelling spatial patterns of fire occurrence [49]. RF is a tree-based ensemble machine learning approach that simultaneously uses multiple decision trees to improve predictive performance [48].

A useful characteristic of RF model is the ability to present the relative importance of each predictor variable. The relative importance was estimated using the "%IncMSE" metric from the RF model. The %IncMSE indicates the mean increase of mean square error in nodes that use any particular variable in the RF model, when values of that variable are randomly permuted [50].

We also used partial dependence analysis and plot (PDP) to show the marginal effect each predictor variable has on the relevant response variable in the RF model. The marginal effect can be interpreted as the expected response, expressed as a function of a given predictor. A PDP can show whether the relationship between the response and a predictor is linear, monotonic, or more complex. PDP and variable importance assessment were both implemented in R (R-Core-Team, 2020), using the "randomForest" and "pdp" package.

### 2.6. Synthetic Minority Over-Sampling Technique

The distribution of observed non-zero PAB values was heavily positively skewed (Fig. S2 online) with comparatively few instances of extreme fire events. This situation caused our RF model to orient itself towards predicting non-extreme events, essentially because such events were overwhelmingly most frequent. However, despite trialling a log transformation of the non-zero PAB data, which is recommended as a first-order correction under skew situations [51], the distribution of observed non-zero PAB values was still very skewed (Fig. S2 online), resulting in a poor goodness-of-fit when we fitted a continuous regression RF model to the data using the full above list of environmental features ($R^2$ was around 0.34, data not shown). To remedy the situation, we transformed all raw non-zero PAB values to resample the rare cases using the Synthetic Minority Over-Sampling Technique (SMOGN) [52,53]. SMOGN has previously been applied to other so-called "imbalanced data" regression problems like ours where the machine learning model was being used to predict extremely rare values of a continuous target variable. A detailed description of the SMOGN technique especially for input parameters can be found in the Python package (https://pypi.org/project/smogn/). The correlation coefficient between PAB and each individual fire weather index was greatly improved after using SMOGN pre-processing (Table S1 online).

### 2.7. Model development

We used Moran's index [54] to test spatial autocorrelation of PAB data over fire grid cells in each month and year. The results show that our PAB data were not independent spatially with Moran's index greater than 0 ($P < 0.01$) for most months and years (Table S2 online). To address the issue of spatial autocorrelation of adjacent fire grids, we used a common way of dealing with this problem by including coordinates (latitude and longitude) as covariates in our model [55,56]. In addition, we observed a significant temporal autocorrelation of PAB with the previous month, but no relationship with two and three months prior (Fig. S3 online). Therefore, we added PAB of the prior month as an additional predictor in models to include temporal inheritance following Song and Wang [57].

We developed four types of RF models by using different groups of fire weather indices, i.e., RF1 based on FWI_mean and FWI_90, RF2 based on DC_mean, DC90, FFMC_mean, and FFMC90, RF3 based on FFDI_mean and FFDI90, and RF4 based on KBDI_mean and KBDI_90. Other predictors including PAB_lag1, NDVI, UW_ratio, F_ratio, Latitude (Lat), and Longitude (Lon) were all the same (Table S3 online). We developed these different RFs because (1) different fire weather indices and their components have different definitions and limitations; (2) some weather indices were highly correlated with each other as they are based on the same climate variables; and (3) we aimed to assess whether these different components of fire weather variability had similar capability to predict forest burnt area. Variables with high multi-collinearity were tested using variable inflation factor (VIF) analyses [58]. All covariates used in each RF model were statistically independent of each other (VIF < 10, Table S3 online).

There are two important parameters in the RF model: (1) number of trees in the forest (ntree) and (2) number of random variables in each tree (mtry). In the RF regression model, the value of mtry commonly used is the number of predictor variables divided by three [59,60], which is the default in the R package of "randomForest". Using a trial and error method to determine the value of mtry, we found that the model accuracy did not increase appreciably compared to that with default mtry. Therefore, we used mtry of 3. We used ntree with 1000 following Ließ et al. [61] and Wang et al. [60]. Same values of mtry and ntree were used for each RF model to avoid any difference in model performance caused by RF parameters.

There were 3635 SMONG data points used for RF model development. We randomly selected 75% of the total dataset for model development, with the remaining 25% used for validation. This calibration and validation procedure was repeated 100 times, applying a sampling with replacement method to obtain 100 random subsamples of the data, each one with its own calibration and validation dataset [39,62]. To evaluate the performance of RF for predicting PAB, we used the two performance measures, coefficient of determination ($R^2$) and relative mean error (RME, %) [63]:

$$R^2 = \left( \frac{\sum_{i=1}^{n}(O_i - \overline{O})(P_i - \overline{P})}{\sqrt{\sum_{i=1}^{n}(O_i - \overline{O})^2}\sqrt{\sum_{i=1}^{n}(P_i - \overline{P})^2}} \right)^2, \quad (1)$$

$$\mathrm{RME}(\%) = \frac{\sum_{i=1}^{n}(O_i - P_i)}{\sum_{i=1}^{n} O_i} \times 100, \quad (2)$$

where $P_i$ and $O_i$ represent the predicted and observed PAB; $\overline{P}$ and $\overline{O}$ represent the means for the predicted and observed PAB and $n$ is the number of samples.

## 3. Results and discussion

### 3.1. The trajectory of the 2019–2020 forest area burnt

Fig. S4 (online) shows the spatial distribution of the forest fires in eastern Australia in the 2019–2020 fire season estimated by MODIS MCD64A1 Burned Area product (accessed on 5th May 2020). As the majority of the burnt area was located in SE Australia, we thus concentrated our study area in NSW, Victoria, and Australian Capital Territory, one of the most fire-prone areas on earth [25]. Fig. 1 shows the evolution of daily burnt area in NSW during the 2019–2020 fire season from 1 September to 29 February, compared with maximum daily values in the previous 20 years. There was already a small peak of BA in early September 2019 when the 2019–2020 fire season started, much earlier than most previous years. The first large peak of around 210, 000 ha occurred on 8 November 2019. Fires then remained very active until late December and daily BA was far higher than the maximum value in previous years. Exacerbated by continuous drought and record-breaking daily heat waves, the second peak with 240,000 ha burnt occurred

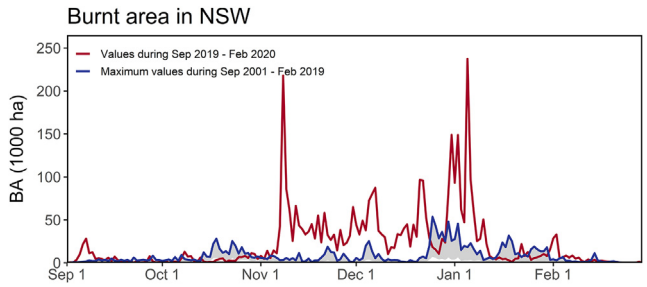


**Fig. 1.** Daily burnt area (BA) in southeast Australian state of New South Wales (NSW) from September 2019 to February 2020, compared to maximum values for that day during the same periods of 2001–2019. The shaded grey area shows the range of mean and maximum daily BA in September-February in 2001–2019. Daily fire data were acquired from MCD64A1 Version 6 Burned Area data products (https://lpdaac.usgs.gov/products/mcd64a1v006/).

on 5 January 2020, four times greater than the daily maximum BA recorded in the 2001–2018 period. Cumulative monthly BA in 2019–2020 showed a dramatic increase after October 2019 (Fig. S5 online). By the end of February 2020, the accumulated BA in NSW was over four times that of the previous record fire (the 2002–2003 fire season) (Fig. S5 online).

### 3.2. Predicting proportion of burnt area at 0.25° grid cell

We developed four types of RF models (RF1-RF4, see model development in Methods) using different sets of environmental covariates (Table S3 online) to estimate the PAB per month, transformed by SMOGN (Fig. S2 online) during October to February at 0.25°. Fig. 2 summarises the results from 100 runs of validating RF model performance. It is worth noting that all RF models yielded similar results. The coefficient of determination ($R^2$) ranged between 0.83 and 0.87 with a relative mean error (RME) of 3.5% to 4.2%. We also built different MLR models to compare their performance with RF. Note that MLR explained at most around 30% of the variance in

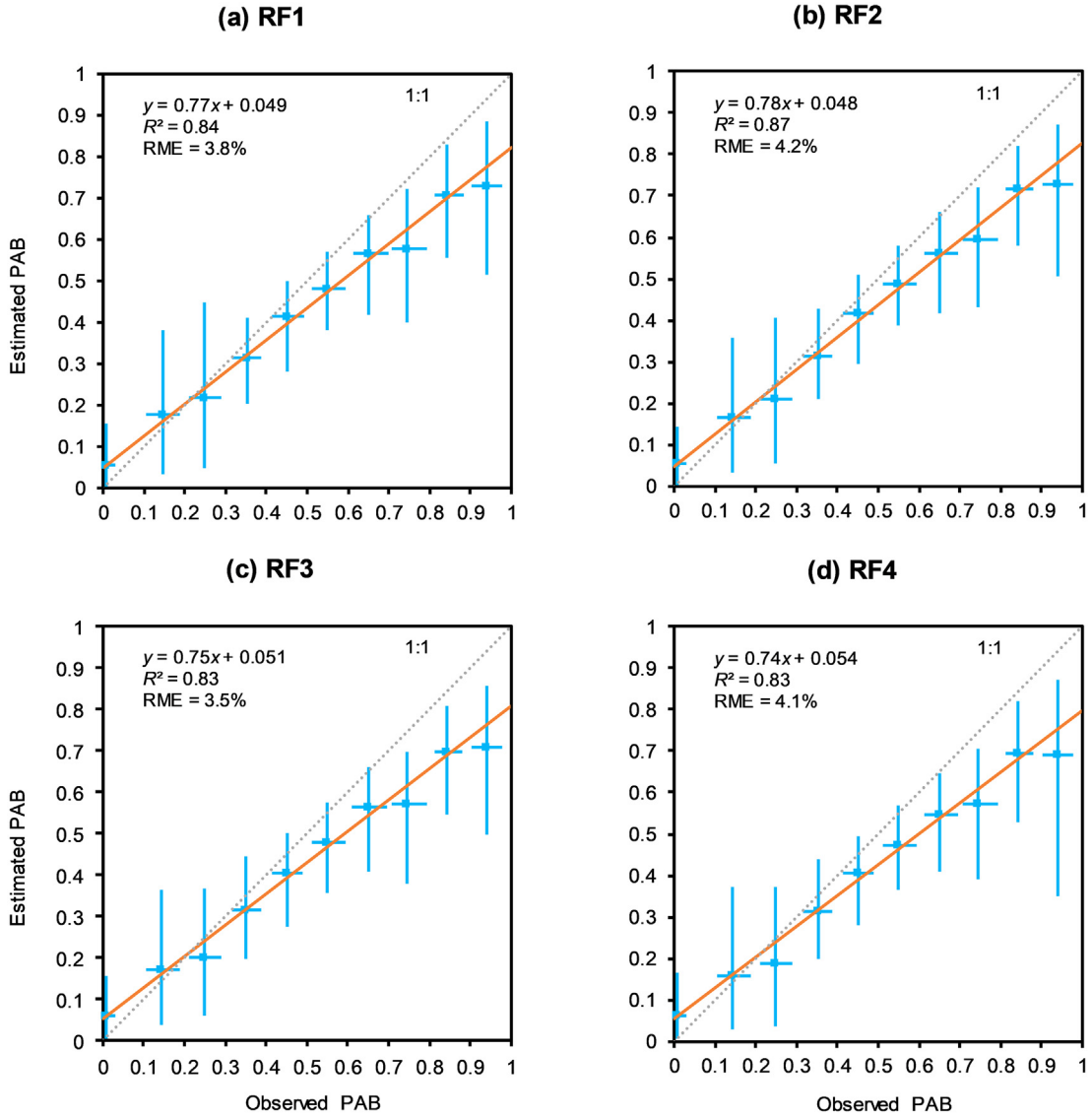


**Fig. 2.** Scatter plot of estimated PAB against observed PAB based on 100 runs of the four types of random forest (RF) models. (a) RF1 based on FWI, (b) RF2 based on DC and FFMC, (c) RF3 based on FFDI, and (d) RF4 based on KBDI. The detailed list of environmental features is shown in Table S3 (online). The orange line represents the fitted line for all validation samples based on 100 runs. To maintain visual clarity, the plot is based on binning of the data along both the *X* and *Y* axes. Specifically, mean observed PAB and mean estimated PAB were calculated at each 0.1 interval or bin along the range [0, 1] (refer blue rectangles). Each blue horizontal line and each blue vertical line represent 10th to 90th percentile range around the mean observed PAB and mean estimated PAB respectively for each bin.

PAB (Fig. S6 online), which was inferior to the RF models. This is because machine learning can simulate both linear and non-linear relationships between fire activity and driving factors [16,18,64].

Our RF model fitting displayed an overall accuracy that is comparable to analogous studies in other forested regions in which monthly burnt area has been regressed as a continuous variable on fire weather conditions [15,65]. However, while the model performed well at intermediate levels of observed burnt area (Fig. 2), it showed some overestimation of PAB where low observed PAB coincided with high FWI (outliers in Fig. S7 online). This discrepancy may be explained by the fact that not all dry forests burn because of other important factors for fire occurrence. For example, an ignition source was lacking, or there was insufficient fuel load due to recent hazard reduction burns or previous wildfires. Additionally, the model tended to underestimate observed burnt area at the high end of the scale (the regression coefficient of estimated on observed burnt area was <1, Fig. 2). Possible causes of this underestimation may stem from the non-linear nature of fire spread under extreme fire weather conditions, which may not be captured by the measures of fire danger indexes and vegetation condition used in this study.

A range of factors not considered in the present study due to insufficient data may explain some of the discrepancies between observed and estimated PAB. Notably, ignition attribution data linking remotely sensed burnt area polygons to either human ignition or dry lightning strikes are lacking, as well as detailed information on the role of barriers to fire spread such as roads, rivers, urban districts, and farmland. Furthermore, our modelling was limited to 0.25° resolution because the fire weather data are based on ERA5 reanalysis data, which are only available at this resolution.

### 3.3. Non-linear relationships between PAB and covariates

Fig. 3 shows the relative importance of explanatory variables in determining PAB. Our model shows that PAB_lag1 (18%) was the most important variable, followed by FWI90 (15.3%), NDVI

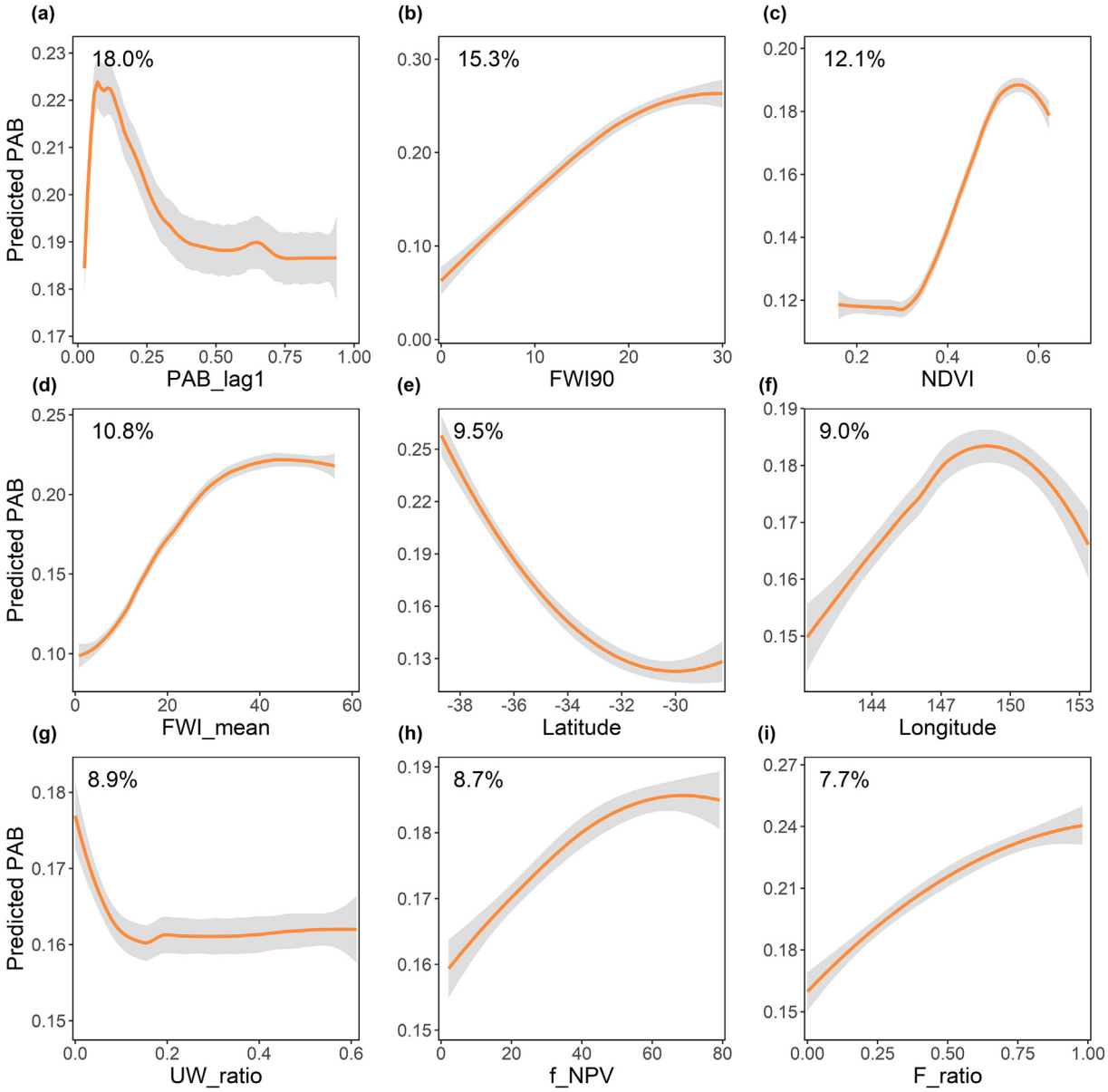


**Fig. 3.** Partial dependence of the proportion of area burnt (PAB) on nine explanatory variables. (a) PAB of prior month, PAB_lag1; (b) the number of days per month that FWI exceeds 90th percentile of daily values, FWI90; (c) median Normalized Difference Vegetation Index, NDVI; (d) the monthly mean of FWI, FWI_mean; (e) latitude; (f) longitude; (g) urban and water ratio, UW_ratio; (h) monthly fractional cover of Non-Photosynthetic Vegetation, f_NPV; (i) forest cover ratio, F_ratio. The percentage values represent the relative importance of each predictor variable based on 100 runs of the Random Forest model. The grey shading area shows the 95% confidence interval.

(12.1%), FWI_mean (10.8%), Latitude (9.5%), Longitude (9.0%), UW_ratio (8.9%), f_NPV (8.7%), and F_ratio (7.7%). Similar results for variable importance were found in the other three types of RF models (Figs. S8–S10 online). Although PAB_lag1 emerged as the most important predictor of PAB, it is challenging to incorporate it as part of future predictive modelling. It should be noted that re-running the RF model with all environmental features except PAB_lag1 could still explain around 76% of the variation in burnt area (data not shown).

A non-linear relationship was detected between PAB of the concurrent month and PAB of the prior month (Fig. 3a). When PAB_lag1 is <0.125, PAB in the target month dramatically increases, which indicates fire persists from the previous month to current month. However, when PAB_lag1 is more than around 0.25, PAB in the current month drops steadily. The impact of fire weather conditions on PAB is clear, evidenced by the strong relationship with FWI90 (Fig. 3b). The effect of previous-years NDVI is non-linear with PAB; there is a peak of PAB when NDVI is around 0.55 (Fig. 3c). This is because higher NDVI has a higher proportion of green vegetation that reduces flammability. Pixels with a longitude of between 147°–150° E and latitude of more than 36° S have a large PAB (Fig. 3e, f). As expected, a high proportion of urban and water areas is associated with reduced area burnt (Fig. 3g) as they break the fuel continuity. The PAB is affected by monthly f_NPV (Fig. 3h) as f_NPV reflects the proportion of area occupied by standing dry vegetation and litter, that determine the fuel state [38]. Landscapes characterised by high forest cover generally possess relatively high fuel loads (e.g., suspended and fallen leaves, branches, bark, and vegetation litter) under dry conditions that readily ignite and spread a wildfire [2,66] (Fig. 3i).

Our results demonstrate the importance of fuel dryness driving PAB variability. The data presented in Fig. S8 (online) show that PAB is slightly more controlled by fluctuations in DC90 and DC_mean than FFMC_mean and FFMC90. The former pair reflect changes in the moisture content of slow-drying larger fuels (branches) and the latter, more rapid changes to moisture content in fine fuels (leaves and twigs) (Section 1 in Supplementary materials). All three fuel types (branches, leaves, and twigs) may influence fire rate of spread and hence burnt area [11,67]. While these fire danger susceptibility indicators are not as sophisticated as more physical-based models of fuel moisture, our results support previous research in forested landscapes demonstrating a close link between large fires and extended previous dry periods that increase the connectivity of available fuels for burning [68].

Further, we considered how two-variable interaction affects PAB under the combination of FWI90 and FWI_mean. As extreme high temperature and low rainfall are favourable conditions for large fires, PAB is greatest when both FWI90 and FWI_mean are high (Fig. S11 online). In addition, using the threshold values between PAB and important predictor variables, we could also identify when and where extreme fires may occur in SE Australia (Fig. S12 online).

If driven by appropriate outputs from seasonal climate forecasts and vegetation models, the non-linear relationships between monthly burnt area and biophysical variables could potentially be adapted for seasonal forecasting of Australian bushfires. The ECWMF SEAS 5 seasonal forecast model [69] is an ideal candidate for seasonal forecasting of climate variables because our study used fire weather indices computed from ECMWF ERA5 reanalysis data to build the PAB model, and ERA5 fields have been used to improve, test, and constrain SEAS5 outputs for Australia [70]. In respect of forecasting vegetation conditions and biomass, the AussieGRASS model [71] would be a good option as it is used for seasonal prediction of vegetation productivity in Australia [72].

### 3.4. Dominant climate mode for fire weather conditions

In SE Australia, three large-scale atmospheric circulation patterns, namely ENSO, SAM, and IOD, are key drivers of seasonal and inter-annual climate patterns [22,73]. Identifying quantitative relationships between fire weather conditions and these climate modes (individually and in combination) can provide useful information to guide effective fire planning and resource management on seasonal timescales and beyond [20]. A positive IOD is typically associated with persistent dry and hot conditions in SE Australia [26], and the 2019–2020 season witnessed one of the strongest positive IOD phases in recent history (Fig. S13b online). By contrast, SAM reached a record low in the 2019–2020 season, the lowest since 2001 (Fig. S13a online). The importance of low SAM values in driving fire activity is highlighted by a recent study showing that in Australia, hot and dry extremes are induced by weakening and warming of the Southern Hemisphere stratospheric polar vortex associated with a negative SAM during the austral spring [74]. The stratospheric vortex was anomalously weak in the middle spring and early summer of 2019 over the South Pole (65°–90°S) (Fig. S14 online). A sudden warming event in the stratosphere (10 hPa) that occurred above Antarctica in September–October (Fig. S14 online) is also likely to have contributed to low rainfall with extreme hot conditions in SE Australia [74]. The El Niño phase of the El Niño-Southern Oscillation (ENSO) characterised by warm sea surface temperatures in the equatorial central-eastern Pacific is also associated with dry conditions in eastern Australia [22]. We used a transformed index based on the regions of Niño4 and Niño3 with conditional constraints to depict central-Pacific El Niño events (CP) [47]. New-record warming CP was observed in this anomalous season (Fig. S13c online) compared to other ENSO indices (Fig. S13d, e online).

Since the FWI and FFDI were highly correlated (Fig. S15 online) [34], we assessed how climate modes influence fire weather conditions by analysing the impacts on FWI only. The concurrent impacts of strongly positive IOD and negative SAM with warmer sea temperature in the central Pacific shifted the FWI towards extremely fire-prone environmental conditions in NSW (Fig. 4). Spatially, FWI90 in spring has a significantly positive relationship with IOD in SE Australia and CP in NSW, whereas it is negatively correlated with SAM ($P < 0.05$) in NSW (Fig. S16 online). This is

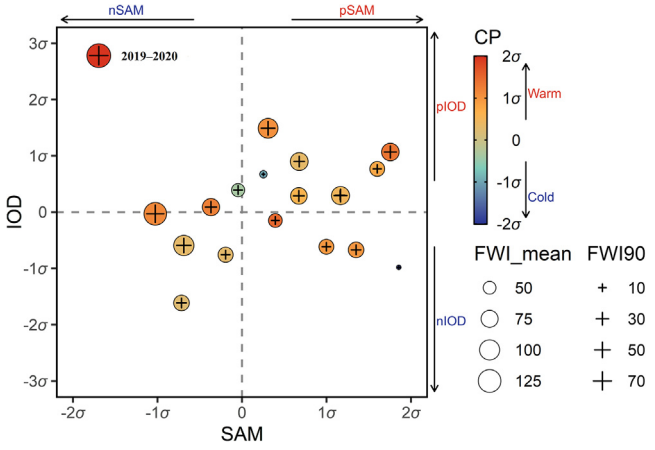


**Fig. 4.** Scatter plot of cumulative monthly fire weather indices FWI_mean and FWI90 in September–February in forested areas of NSW for the past 20 years (2001–2020) against the SAM, IOD, and central Pacific El Niño (CP). The three climate drivers are shown as cumulative values from September to February and are all normalized. The Indian Ocean Dipole (IOD) is measured by the Dipole Mode Index, SAM is an observation-based Southern Hemisphere Annular Mode Index, and CP is the central Pacific El Niño transformed by Niño4 and Niño3 indices [47].

consistent with Harris and Lucas [20] showing that the SAM primarily influences fire weather in late-winter and spring. By contrast, for summer, only CP is significantly related to FWI90 over a substantial area of NSW, while the impact of SAM is restricted to southeast NSW and a small region on the eastern border of NSW and Victoria is affected by IOD (Fig. S16 online). Similar results can be seen for FWI_mean (Fig. S17 online).

Further analyses of FWI-driver dynamics were conducted to (1) identify the contribution of individual large-scale climate modes influencing FWI90; and (2) assess non-linear relationships between climate modes and FWI90. We found that SAM (49.3%) and IOD (47.2%) are the dominant climate drivers affecting FWI90 in forest areas, followed by the CP El Niño index (3.5%) (Fig. 5). Similar results were found for FWI_mean (Fig. S18 online). This differs from previous studies reporting ENSO and IOD as the predominant drivers of interannual fire weather conditions in SE Australia, using correlation-based analysis [20,29,75,76]. The individual single-variable partial dependence plot shows that when the value of SAM is less than around $-0.5\sigma$, the FWI90 increases sharply (Fig. 5a). It is evident that high FWI90 occurs under the positive phase of IOD, especially when IOD is more than $1\sigma$ (Fig. 5b). Meanwhile, FWI90 increases markedly when CP exceeds around $0.5\sigma$ (Fig. 5c). These fire weather threshold values identified for each climate mode provide an important evidence-based guide for pre-empting extreme fire weather events for an upcoming fire season. Further, we examined how two-variable interaction affects the predictions of FWI90 under different combinations of IOD, SAM, and CP. Fig. 5d–f shows the interactive effects of each pair of drivers (IOD vs SAM, IOD vs CP, and SAM vs CP) on FWI90. SAM mainly showed first-order effects on FWI90 irrespective of IOD and CP (Fig. 5d, f) as SAM had dominant effects on FWI90 (Fig. 5a); significant interaction was only seen between CP and IOD (Fig. 5e).

## 4. Conclusion

We used RF modelling to quantify important non-linear relationships between burnt area and a suite of key geographic and bioclimatic explanatory variables in SE Australian forests (2001–2020). Using multiple explanatory variables with different fire weather indices, the RF models performed well in estimating monthly burnt area with an overall accuracy of 83%–87%. We found that large burnt areas were associated with elevated values of fire weather indices (e.g., FWI_mean and FWI90) and regions with high forest cover and low water/urban cover. RF model can improve our understanding of the response of burnt area to each predictor variable based on threshold values.

The RF model simulating FWI as a function of climate modes identified non-linear relationships and thresholds in extreme fire weather with respect to changes in major climate modes. Australia's climate is projected to become hotter and drier under global warming, with extreme fire seasons such as the 2019–2020 season likely to become more frequent in future. Furthermore, much of the projected change in southeast Australia's climate is forecast to occur through an increased frequency of the phases of the three major climate modes leading to drought events, viz., El Niño, positive IOD, and negative SAM.

As our RF model performs well in estimating PAB, it could be used by fire-fighting and forest conservation agencies to compute the likely monthly burnt area at 0.25° resolution, up to several

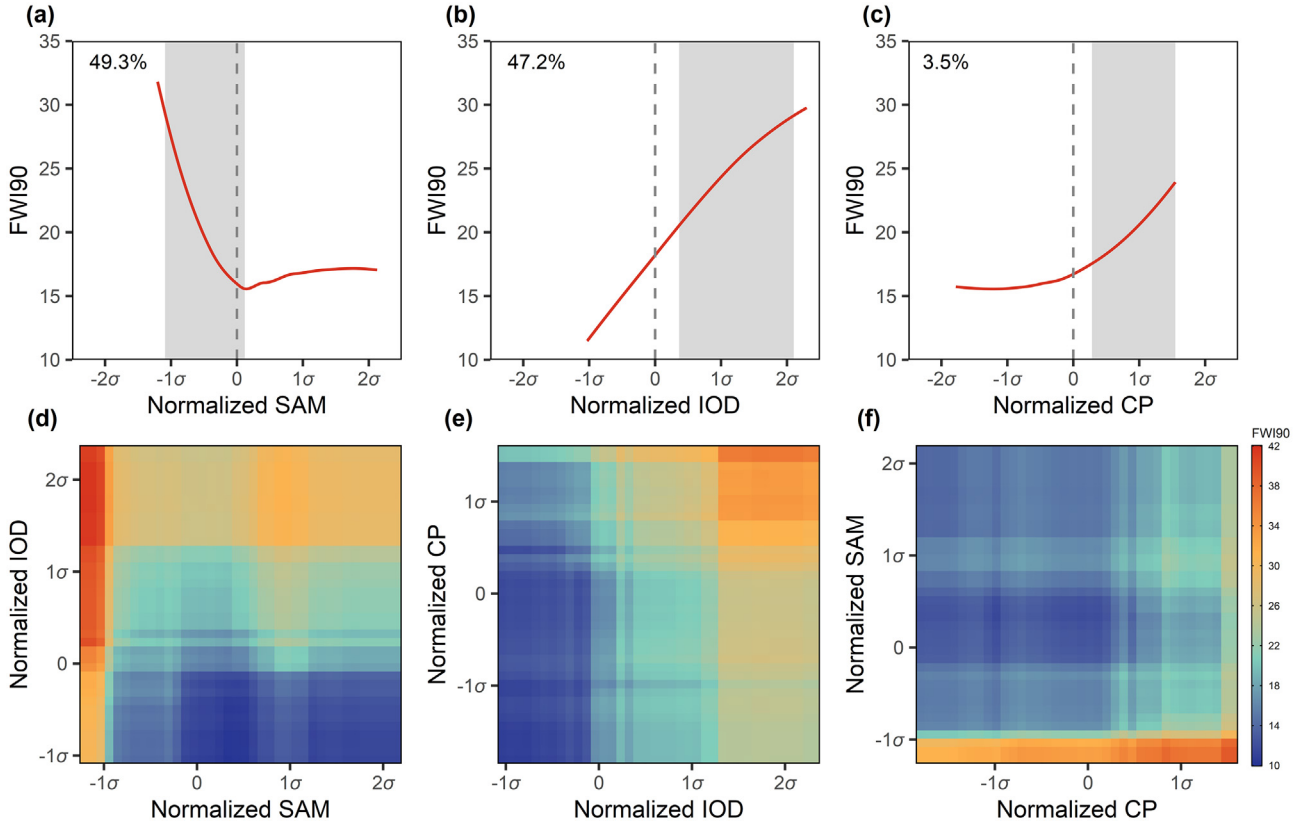


**Fig. 5.** Partial dependence of FWI90 (days) on the three climate modes of SAM (a), IOD (b), and central Pacific El Niño (CP) (c). The percentage values denote the relative importance of each driver as identified by the random forest model. The trend of the red line describes the nature of the dependence between the response and predictors. The shaded area indicates the range of each driver during November 2019–January 2020. We also made partial dependence plots of FWI90 for combined values of the two-variable drivers (d–f).

months in advance. Specifically, when seasonal forecast climate data and forecasts of vegetation condition and biomass are available for the upcoming fire season, these agencies could use those forecast data as inputs to our RF model to estimate burnt area for any given target month based on the forecast values of environmental variables during the concurrent month. In summary, an early fire warning system would assist efforts to advance proactive fire management in Australian forests including the deployment of fire-fighting resources well ahead of potentially hazardous fire conditions.

## Conflict of interest

The authors declare that they have no known conflict of interest.

## Acknowledgments

This work was supported by the National Natural Science Foundation of China (42088101 and 42030605). We are grateful to the ECMWF (European Centre for Medium-Range Weather Forecasts) for providing freely available historical fire weather indices via the Copernicus Data server as part of the Copernicus Emergency Management Service. Allan Spessa and Tadas Nikonovas appreciate support from the research project: Towards an Operational Fire Early Warning System for Indonesia (TOFEWSI). The TOFEWSI project was funded from October 2017–October 2021 through the UK's National Environment Research Council/Newton Fund on behalf of the UK Research & Innovation (NE/P014801/1) (UK Principal Investigator: Allan Spessa) (https://tofewsi.github.io/). Xiaowei Guo receives financial support from the Natural Science Foundation of Qinghai (2021-HZ-811). We thank Dr. Sarah Harris from Bushfire Management Country Fire Authority and two anonymous reviewers for their helpful comments to improve the manuscript.

## Appendix A. Supplementary materials

Supplementary materials to this article can be found online at https://doi.org/10.1016/j.scib.2021.10.001.

## References

[1] Giglio L, Boschetti L, Roy DP, et al. The collection 6 modis burned area mapping algorithm and product. Remote Sens Environ 2018;217:72–85.
[2] Williams RJ, Gill AM, Bradstock RA. Flammable Australia: fire regimes, biodiversity and ecosystems in a changing world. Collingwood: CSIRO Publishing; 2012.
[3] Beringer J, Hutley LB, Abramson D, et al. Fire in Australian savannas: from leaf to landscape. Glob Change Biol 2015;21:62–81.
[4] Phillips N, Nogrady B. The race to decipher how climate change influenced Australia's record fires. Nature 2020;577:610–2.
[5] Bureau of Meteorology. Special climate statement 70-drought conditions in eastern Australia and impact on water resources in the murray-darling basin. 2019, http://www.Bom.Gov.Au/climate/current/statements/scs70a.Pdf.
[6] Woinarski J, Wintle B, Dickman C, et al. A season in hell: bushfires push at least 20 threatened species closer to extinction. 2020, https://theconversation.Com/a-season-in-hell-bushfires-push-at-least-20-threatened-species-closer-to-extinction-129533..
[7] Sanderson BM, Fisher RA. A fiery wake-up call for climate science. Nat Clim Chang 2020;10:175–7.
[8] Australian Government Department of Industry, Science, Energy and Resources. National greenhouse gas inventory report 2018. 2020, https://www.Industry.Gov.Au/data-and-publications/national-greenhouse-gas-inventory-report-2018.
[9] Boer MM, de Dios VR, Bradstock RA. Unprecedented burn area of Australian mega forest fires. Nat Clim Chang 2020;10:171–2.
[10] Nolan RH, Boer MM, Collins L, et al. Causes and consequences of eastern Australia's 2019–20 season of mega-fires. Glob Change Biol 2020;26:1039–41.
[11] Hantson S, Arneth A, Harrison SP, et al. The status and challenge of global fire modelling. Biogeosciences 2016;13:3359–75.
[12] Syphard AD, Keeley JE, Pfaff AH, et al. Human presence diminishes the importance of climate in driving fire activity across the united states. Proc Natl Acad Sci USA 2017;114:13750–5.
[13] Lucas TCD. A translucent box: interpretable machine learning in ecology. Ecol Monogr 2020;90:e01422.
[14] Jain P, Coogan SCP, Subramanian SG, et al. A review of machine learning applications in wildfire science and management. Environ Rev 2020;28:478–505.
[15] Amatulli G, Camia A, San-Miguel-Ayanz J. Estimating future burned areas under changing climate in the EU-Mediterranean countries. Sci Total Environ 2013;450-451:209–22.
[16] Ma W, Feng Z, Cheng Z, et al. Identifying forest fire driving factors and related impacts in China using random forest algorithm. Forests 2020;11:507.
[17] Dutta R, Das A, Aryal J. Big data integration shows Australian bush-fire frequency is increasing significantly. R Soc Open Sci 2016;3:150241.
[18] Clarke H, Penman T, Boer M, et al. The proximal drivers of large fires: a pyrogeographic study. Front Earth Sci 2020;8:90.
[19] Clarke H, Lucas C, Smith P. Changes in Australian fire weather between 1973 and 2010. Int J Climatol 2013;33:931–44.
[20] Harris S, Lucas C, Ummenhofer C. Understanding the variability of Australian fire weather between 1973 and 2017. PLoS One 2019;14:e0222328.
[21] The Commonwealth Scientific and Industrial Research Organisation, Bureau of Meteorology. Climate change in Australia information for Australia's natural resource management regions. Technical Report; 2015.
[22] Risbey JS, Pook MJ, McIntosh PC, et al. On the remote drivers of rainfall variability in Australia. Mon Weather Rev 2009;137:3233–53.
[23] Nolan RH, Blackman CJ, de Dios VR, et al. Linking forest flammability and plant vulnerability to drought. Forests 2020;11:779.
[24] Cai W, Cowan T, Raupach M. Positive indian ocean dipole events precondition southeast Australia bushfires. Geophys Res Lett 2009;36:L19710.
[25] Mariani M, Fletcher M-S, Holz A, et al. Enso controls interannual fire activity in southeast Australia. Geophys Res Lett 2016;43:10891–900.
[26] Ummenhofer CC, England MH, McIntosh PC, et al. What causes southeast Australia's worst droughts? Geophys Res Lett 2009;36:L04706.
[27] Cai W, Santoso A, Wang G, et al. Increased frequency of extreme Indian Ocean dipole events due to greenhouse warming. Nature 2014;510:254–8.
[28] Cai W, Wang G, Dewitte B, et al. Increased variability of eastern Pacific El Niño under greenhouse warming. Nature 2018;564:201–6.
[29] Dowdy AJ. Climatological variability of fire weather in Australia. J Appl Meteorol Climatol 2017;57:221–34.
[30] Abram NJ, Henley BJ, Sen Gupta A, et al. Connections of climate change and variability to large and extreme forest fires in southeast Australia. Commun Earth Environ 2021;2:8.
[31] Kganyago M, Shikwambana L. Assessment of the characteristics of recent major wildfires in the USA, Australia and Brazil in 2018–2019 using multi-source satellite products. Remote Sens 1803;12:1803.
[32] Seydi ST, Akhoondzadeh M, Amani M, et al. Wildfire damage assessment over Australia using sentinel-2 imagery and modis land cover product within the google earth engine cloud platform. Remote Sens 2021;13:220.
[33] Van Wagner C. Development and structure of the Canadian forest fire weather index system. Ottawa: Canadian Forestry Service; 1987.
[34] Dowdy AJ, Mills GA, Finkele K, et al. Australian fire weather as represented by the mcarthur forest fire danger index and the canadian forest fire weather index. Melbourne, Australia: Techical Report. Centre for Australian Weather and Climate Research; 2009.
[35] Noble IR, Gill AM, Bary GAV. Mcarthur's fire-danger meters expressed as equations. Aust J Ecol 1980;5:201–3.
[36] Vitolo C, Di Giuseppe F, Barnard C, et al. ERA5-based global meteorological wildfire danger maps. Sci Data 2020;7:216.
[37] Varga TA, Asner GP. Hyperspectral and lidar remote sensing of fire fuels in Hawaii Volcanoes National Park. Ecol Appl 2008;18:613–23.
[38] Guerschman JP, Scarth PF, McVicar TR, et al. Assessing the effects of site heterogeneity and soil properties when unmixing photosynthetic vegetation, non-photosynthetic vegetation and bare soil fractions from landsat and modis data. Remote Sens Environ 2015;161:12–26.
[39] Wang B, Waters C, Orgill S, et al. High resolution mapping of soil organic carbon stocks using remote sensing variables in the semi-arid rangelands of eastern Australia. Sci Total Environ 2018;630:367–78.
[40] Zhang Y, Lim S, Sharples JJ. Wildfire occurrence patterns in ecoregions of new south wales and Australian capital territory. Australia. Nat Hazards 2017;87:415–35.
[41] Turner D, Lewis M, Ostendorf B. Spatial indicators of fire risk in the arid and semi-arid zone of Australia. Ecol Indic 2011;11:149–67.
[42] le Maire G, Marsden C, Nouvellon Y, et al. Modis ndvi time-series allow the monitoring of eucalyptus plantation biomass. Remote Sens Environ 2011;115:2613–25.
[43] Guerschman JP, Hill MJ, Leys J, et al. Vegetation cover dependence on accumulated antecedent precipitation in Australia: relationships with photosynthetic and non-photosynthetic vegetation fractions. Remote Sens Environ 2020;240:111670.
[44] Marshall GJ. Trends in the southern annular mode from observations and reanalyses. J Clim 2003;16:4134–43.
[45] Chiew FHS, Piechota TC, Dracup JA, et al. El Niño/southern oscillation and Australian rainfall, streamflow and drought: links and potential for forecasting. J Hydrol 1998;204:138–49.
[46] Yeh S-W, Kug J-S, Dewitte B, et al. El Niño in a changing climate. Nature 2009;461:511–4.
[47] Sullivan A, Luo J-J, Hirst AC, et al. Robust contribution of decadal anomalies to the frequency of central-Pacific El Niño. Sci Rep 2016;6:38540.

[48] Breiman L. Random forests. Mach Learn 2001;45:5–32.
[49] Oliveira S, Oehler F, San-Miguel-Ayanz J, et al. Modeling spatial patterns of fire occurrence in Mediterranean Europe using multiple regression and random forest. Forest Ecol Manage 2012;275:117–29.
[50] Feng P, Wang B, Liu DL, et al. Impacts of rainfall extremes on wheat yield in semi-arid cropping systems in eastern Australia. Clim Change 2018;147:555–69.
[51] Turco M, von Hardenberg J, AghaKouchak A, et al. On the key role of droughts in the dynamics of summer fires in Mediterranean Europe. Sci Rep 2017;7:81.
[52] Branco P, Torgo L, Ribeiro RP. SMOGN: a pre-processing approach for imbalanced regression. In: Proceedings of the First International Workshop on Learning with Imbalanced Domains: Theory and Applications 2017;74:36–50.
[53] Janković R, Mihajlović I, Štrbac N, et al. Machine learning models for ecological footprint prediction based on energy parameters. Neural Comput Appl 2021;33:7073–87.
[54] Moran PAP. Notes on continuous stochastic phenomena. Biometrika 1950;37:17–23.
[55] Ahn S, Ryu D-W, Lee S. A machine learning-based approach for spatial estimation using the spatial features of coordinate information. ISPRS Int J Geo-Inf 2020;9:587.
[56] Behrens T, Schmidt K, Viscarra Rossel RA, et al. Spatial modelling with euclidean distance fields and machine learning. Eur J Soil Sci 2018;69:757–70.
[57] Song Y, Wang Y. Global wildfire outlook forecast with neural networks. Remote Sens 2020;12:2246.
[58] Scheller RM, Mladenoff DJ. Simulated effects of climate change, fragmentation, and inter-specific competition on tree species migration in northern wisconsin, USA. Clim Res 2008;36:191–202.
[59] Were K, Bui DT, Dick ØB, et al. A comparative assessment of support vector regression, artificial neural networks, and random forests for predicting and mapping soil organic carbon stocks across an afromontane landscape. Ecol Indic 2015;52:394–403.
[60] Wang B, Feng P, Waters C, et al. Quantifying the impacts of pre-occurred enso signals on wheat yield variation using machine learning in Australia. Agric For Meteorol 2020;291:108043.
[61] Ließ M, Schmidt J, Glaser B, et al. Improving the spatial prediction of soil organic carbon stocks in a complex tropical mountain landscape by methodological specifications in machine learning approaches. PLoS One 2016;11:e0153673.
[62] Gomes LC, Faria RM, de Souza E, et al. Modelling and mapping soil organic carbon stocks in Brazil. Geoderma 2019;340:337–50.
[63] Miehle P, Battaglia M, Sands PJ, et al. A comparison of four process-based models and a statistical regression model to predict growth of eucalyptus globulus plantations. Ecol Model 2009;220:734–46.
[64] Su Z, Hu H, Wang G, et al. Using gis and random forests to identify fire drivers in a forest city, Yichun, China. Geomat Nat Hazards Risk 2018;9:1207–29.
[65] Turco M, Jerez S, Doblas-Reyes FJ, et al. Skilful forecasting of global fire activity using seasonal climate predictions. Nat Commun 2018;9:2718.
[66] Bradstock RA. A biogeographic model of fire regimes in Australia: current and future implications. Glob Ecol Biogeogr 2010;19:145–58.
[67] Rabin SS, Melton JR, Lasslop G, et al. The fire modeling intercomparison project (firemip), phase 1: experimental and analytical protocols with detailed model descriptions. Geosci Model Dev 2017;10:1175–97.
[68] Nolan RH, Boer MM, de Dios VR, et al. Large-scale, dynamic transformations in fuel moisture drive wildfire activity across southeastern Australia. Geophys Res Lett 2016;43:4229–38.
[69] Johnson SJ, Stockdale TN, Ferranti L, et al. SEAS5: the new ECMWF seasonal forecast system. Geosci Model Dev 2019;12:1087–117.
[70] Wang QJ, Shao Y, Song Y, et al. An evaluation of ECMWF SEAS5 seasonal climate forecasts for Australia using a new forecast calibration algorithm. Environ Model Softw 2019;122:104550.
[71] Carter J, Hall W, Brook K, et al. Aussie grass: Australian grassland and rangeland assessment by spatial simulation. In: Hammer GL, Nicholls N, Mitchell C, editors. Applications of seasonal climate forecasting in agricultural and natural ecosystems. Berlin: Springer; 2000. p. 329–49.
[72] Stone G, Pozza RD, Carter J, et al. Long paddock: climate risk and grazing information for Australian rangelands and grazing communities. Rangel J 2019;41:225.
[73] Cai W, van Rensch P, Cowan T, et al. Teleconnection pathways of ENSO and the iod and the mechanisms for impacts on Australian rainfall. J Clim, 2011, 24: 3910-3923.
[74] Lim E-P, Hendon HH, Boschat G, et al. Australian hot and dry extremes induced by weakenings of the stratospheric polar vortex. Nat Geosci 2019;12:896–901.
[75] Verdon DC, Kiem AS, Franks SW. Multi-decadal variability of forest fire riskeastern Australia. Int J Wildland Fire 2004;13:165.
[76] Williamson GJ, Prior LD, Jolly WM, et al. Measurement of inter- and intra-annual variability of landscape fire activity at a continental scale: the Australian case. Environ Res Lett 2016;11:035003.

Bin Wang is a research scientist at Wagga Wagga Agricultural Institute, New South Wales Department of Primary Industries, Australia. He received his Bachelor of Science degree from Nanjing Agricultural University (2010) and Ph.D. degree from University of Technology Sydney (2017). His research interest focuses on using process-based biophysical model and statistical model (e.g., machine learning) to assess the impacts of climate change on agriculture, forestry, and hydrology.

Jing-Jia Luo got his Ph.D. degree of physical oceanography at Tokyo University in 2001, and then joined Japan Agency for Marine-Earth Science and Technology from 2001 to 2011 and Australian Bureau of Meteorology during 2011–2018. Since 2018, he has acted as professor & director at Institute for Climate and Application Research, Nanjing University of Information Science and Technology. His research interest includes climate dynamics, model development, climate prediction and application.

Qiang Yu is a lead professor in the State Key Laboratory of Soil Erosion and Dryland Farming on the Loess Plateau, Northwest A&F University. He is also a professor of the University of Chinese Academy of Sciences. He received his Ph.D. degree of climatology at Nanjing University in 1994. His research interest includes crop modelling, ecosystem ecology, climate change impacts, and digital agriculture.